Uhland et al. *EPJ Quantum Technology* (2015) 2:20
DOI 10.1140/epjqt/s40507-015-0033-1

EPJ Quantum Technology
a SpringerOpen Journal

EPJ.org

RESEARCH Open Access

Single molecule DNA detection with an atomic vapor notch filter

Denis Uhland[1], Torsten Rendler[1], Matthias Widmann[1], Sang-Yun Lee[1], Jörg Wrachtrup[1,2] and Ilja Gerhardt[1,2*]

*Correspondence:
i.gerhardt@fkf.mpg.de
[1]3rd Physics Institute, University of Stuttgart and Stuttgart Research Center of Photonic Engineering (SCoPE) and IQST, Pfaffenwaldring 57, Stuttgart, 70569, Germany
[2]Max Planck Institute for Solid State Research, Heisenbergstraße 1, Stuttgart, 70569, Germany

Abstract

The detection of single molecules has facilitated many advances in life- and material-science. Commonly the fluorescence of dye molecules is detected, which are attached to a non-fluorescent structure under study. For fluorescence microscopy one desires to maximize the detection efficiency together with an efficient suppression of undesired laser leakage. Here we present the use of the narrow-band filtering properties of hot atomic sodium vapor to selectively filter the excitation light from the red-shifted fluorescence of dye labeled single-stranded DNA molecules. A statistical analysis proves an enhancement in detection efficiency of more than 15% in a confocal and in a wide-field configuration.

Keywords: DNA detection; fluorescence microscopy; single molecules; atomic filtering; sodium spectroscopy

1 Introduction

The optical detection of single molecules [1–3] has facilitated important progress in various fields of research. Especially in microbiology the localization and tracking of labeled biomolecules [4–6] or other relevant structures like DNA molecules [7–10] reveals underlying compositions and functionalities of living cells. Normally the red-shifted fluorescence of single molecule labels is detected. Besides probe specific properties like the (non-)radiative decay rate of the involved electronic transitions also experimental parameters like sample absorption, collection and detection efficiency of the given setup determine the number of detectable photons. Under ambient conditions the total number of emitted photons of an organic fluorophore is limited by photo-bleaching [11]. This poses a serious problem, since parameters such as the localization accuracy are limited by the finite number of detected photons. In single molecule studies the precision is usually shot-noise limited, scaling as $1/\sqrt{N}$, where N is the total number of detected photons. Once a fluorescent dye is chosen there remain two key parameters to optimize: The collection and detection efficiency of the microscope.

In the last decade there have been many efforts to optimize all involved experimental parameters. For example photo-stable alternatives to dyes like defect centers in diamond [12, 13] and semiconductor nano-crystals [14] were investigated. Non-fluorescent structures can be detected with a high signal-to-noise ratio [15], or novel techniques extract a higher amount of information from an acquired image [16]. Other attempts have been made to

increase the extraction efficiency from the structure under study [17, 18]. Additionally, the detectors have been continuously improved, such that nowadays silicon avalanche photon diodes (APDs) exhibit more than 70% quantum efficiency in the range of 650-750 nm and sensitive CCD-cameras more than 95% from 500-650 nm. Another way to enhance the overall detection efficiency is an optimized filtering scheme. An ideal filter solely blocks the excitation light which is scattered by the sample and transmits all photons originated by fluorescence. The edge-steepness should be ideally a step-function as sharp as the spectra laser line, but is often limited by material properties and technical imperfections to some nanometers which are common in dichroic mirrors and filters.

Hot atomic vapors can also allow for optical filtering. These are generally easy to handle in evacuated glass reference cells. They are typically composed of an evacuated glass cylinder with optical windows, in which a small amount of alkali metals (hundreds of milligram) is present. Such cells can exhibit a large optical depth and simultaneously ensure a few GHz spectral width. The optical rejection obeys Beer-Lambert's law and is a function of the vapor density, which rises approximately exponentially with temperature. The spectral width is to a first approximation given by the Doppler broadening of an atomic vapor in the range of a few GHz at ambient conditions up to a few hundred degree centigrade [19]. In atom optics experiments such filtering schemes are common and have been characterized for different alkali metals like rubidium [20, 21]. One common use is to filter the emission of one isotope of rubidium with another, an application which is commonly implemented in atomic clocks [22]. These filters are also suitable for other applications like Raman spectroscopy [23–26] and are intrinsically matched to atomic transitions.

Here we compare the filtering performance of a high-end commercial filter with a hot atomic sodium vapor cell in context of detection of single fluorescing molecules in a confocal [27] and a wide-field microscope [28]. Unlike many other atomic filters, sodium matches the visible range of many common dye systems which are used for biological labeling. For this demonstration we study single stranded DNA molecules, labeled with a commonly used fluorescent dye (Atto 590, ATTO-TEC). Both microscopic schemes, confocal and wide-field, have their specific advantages and disadvantages. We show that filtering with atomic vapor is able to facilitate an enhanced detection of the fluorescence which originates from a single molecule. The first steps of this study were presented for single molecules under cryogenic conditions [29], and in a micro-fluidic configuration [30].

2 Experimental configuration

The experimental configuration consists of a combined confocal and wide-field microscope (Figure 1(b)). Both experimental configurations are described below. Filtering is performed with a commercial filter and an atomic vapor cell.

2.1 Excitation laser

The excitation laser is a dye ring laser (699-21, Coherent), which can be locked to a sodium transition. The lock-signal is provided by Doppler-free dichroic atomic vapor laser lock (DAVLL, see e.g. [31]) with a 140°C hot sodium vapor cell. For optimal optical rejection the laser is locked to the cross-over resonance, midway between the two $F = 1$ and $F = 2$ ground states of the D_2-line (see Figure 1(d)). This defines for further filtering purposes a preferred point, since both optical transitions add up due to their Doppler broadening.

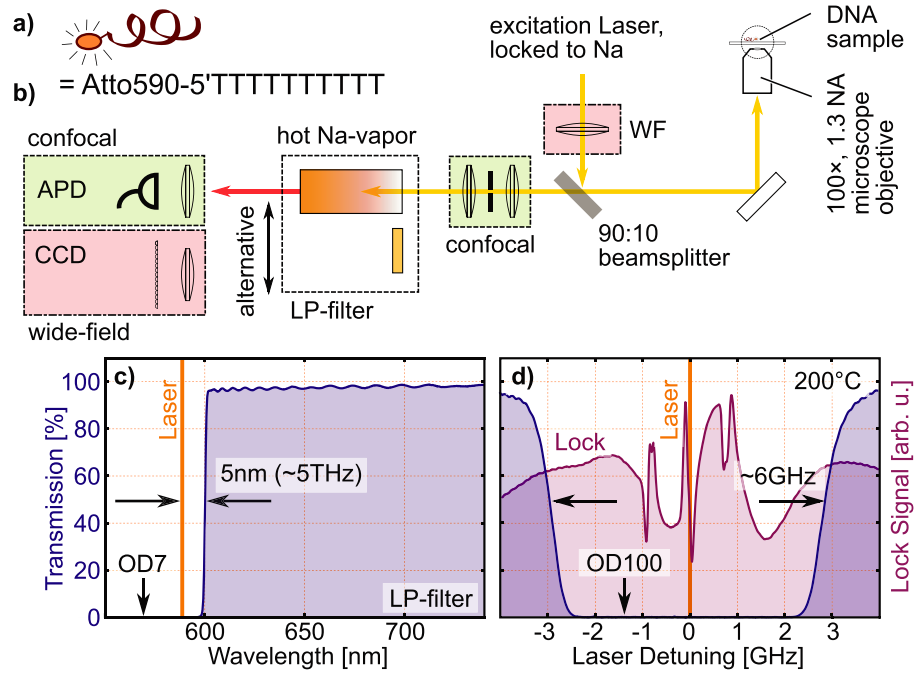

Figure 1 Experimental configuration. (a) Single stranded DNA under study, labeled at the 5'-end with the organic dye 'Atto590'. **(b)** Confocal and wide-field microscope. The filter configuration can be changed in approx. 1 s. WF = wide-field configuration; APD = avalanche photo diode; LP-filter = long-pass filter; CCD = charged coupled device, camera; **(c)** Laser emission and filter function of the commercial long pass filter. OD = optical density; **(d)** Spectrum of the sodium reference cell scanning over the D_2 resonance frequency. The purple line shows the Doppler-free difference laser lock signal. The blue line shows the measured absorption spectrum of the atomic vapor cell at 200°C. The block band is approx. 6 GHz broad and shows an optical rejection of more than 6 orders of magnitude (measured). The calculated optical density is much higher (OD 100).

Note, that this zero-point does not represent the 'center of gravity' of the unshifted sodium transition. The dispersive lock signal depicted in Figure 1(d) is robust against external influences such as mechanical noise on the laser table. For the rare case the laser jumps out of lock, the signal is monitored with an oscilloscope (LeCroy, WavePro 7K), where the pass-fail output controls an optical shutter and blocks the laser if required to prevent damage to the used single photon detector. A 20 m long optical single mode glass fiber guides the laser beam to the setup. The light is then filtered with a narrow band-pass filter (589 ± 0.2 nm, Omega Optical), since our analysis showed that we can further suppress the background level (data not shown). The microscope is built around a commercial inverted microscope (Olympus IX71). In both configurations the sample is excited and detected via a $100\times$, 1.3 NA microscope objective (UPLANFL, Olympus).

2.2 Confocal microscope

For the confocal configuration, the collimated beam is reflected into the microscope via a quartz wedge (10% reflectivity). This is not realized by a dichroic beam-splitter to avoid additional spectral cut-off of the detected fluorescence signal. The light is focused onto and collected from the sample with the microscope objective. Spatial discrimination is performed by focusing the resulting beam onto a 50 µm sized pinhole. From there, it is again 1:1 collimated and passes through the laser suppression filter under study. The fil-

tered light is then focused onto a single photon counting module (SPCM-AQR-14, Excelitas). Addressing different locations on the sample and focusing is realized by scanning the sample with a 3D-piezo actuator (P527.3CL, Physik Instrumente). A pixel size of 100 nm was used with a typical integration time of 10 ms per pixel. The entire detection scheme is carefully optically shielded from the environment.

To acquire single molecule spectra, a flip-mirror is introduced into the confocal configuration to divert the light from the single photon detector to a Peltier cooled CCD spectrometer (Princeton Instruments, Acton, 300 mm, camera: 'Pixis'). An acquisition time of 30 s is used.

2.3 Wide-field microscope

For the wide-field microscope experiments, the incident laser light is focused by a pair of achromatic lenses (100 mm and 50 mm focal length) into the back-focal plane of the microscope objective. The resulting illuminated area in the objective plane is 25 μm in diameter. For imaging, a Peltier cooled CCD camera is used (Photometrics Cascade 512B) with a pixel size of 16×16 μm^2 and 512×512 pixels. The objective plane is projected via a 250 mm achromatic lens onto the CCD chip. As a consequence one pixel represents a 115×115 nm^2 sized area on the sample. A typical acquisition was performed with an exposure time of 10 s and no internal gain. For comparison between the two microscope configurations we convert the output by the camera, which is give in analog-digital units (ADUs) to an incident photon equivalent onto the CCD chip. In the used configuration 4 detected photons correspond to 1 ADU.

2.4 The sample

The single stranded deoxyribonucleic acid (DNA) under study consists of 10 bases (5′-TTTTTTTTTT, see also Figure 1(a)) and is labeled on the 5′-end with Atto 590 (Thermo Scientific). This dye is a common dye label in micro-biology, which spectral matches to atomic sodium vapor. The sample is produced by first dissolving and diluting the dried DNA in sterile water. Then, an aqueous polyvinyl alcohol (PVA) solution (3 mg/ml) is stepwise mixed with the DNA solution until a relative DNA concentration of 1:10^{14}-1:10^{15} is reached. Finally the mixture is spin-coated onto a nitrogen-plasma cleaned cover slides. For most of the experiments a concentration of 1:10^{15} was used because it results in single molecules separated by several μm, whereas the 1:10^{14} diluted sample shows a too dense concentration for our automated peak-finding routine. The thickness of the sample has been calculated to be below 1 μm.

To verify that the experiments are performed on the single molecule level, the typical blinking behavior of single molecules is confirmed in the wide-field configuration with millisecond integration times. In the confocal configuration single step bleaching around $t = 500$ s can be seen as shown in Figure 2(b), which is used for the verification of single molecules. Note, that no telegraph function or triplet blinking is observed during this acquisition.

2.5 Filtering the excitation light

The optical filtering from the microscope is performed with two possible filter configurations: a commercial filter and an atomic sodium vapor cell.

The commercial filter (Semrock, FF01-593/LP-25) efficiently rejects the excitation light and exhibits around 97% transmission in its pass-band. A spectrum of the filter was

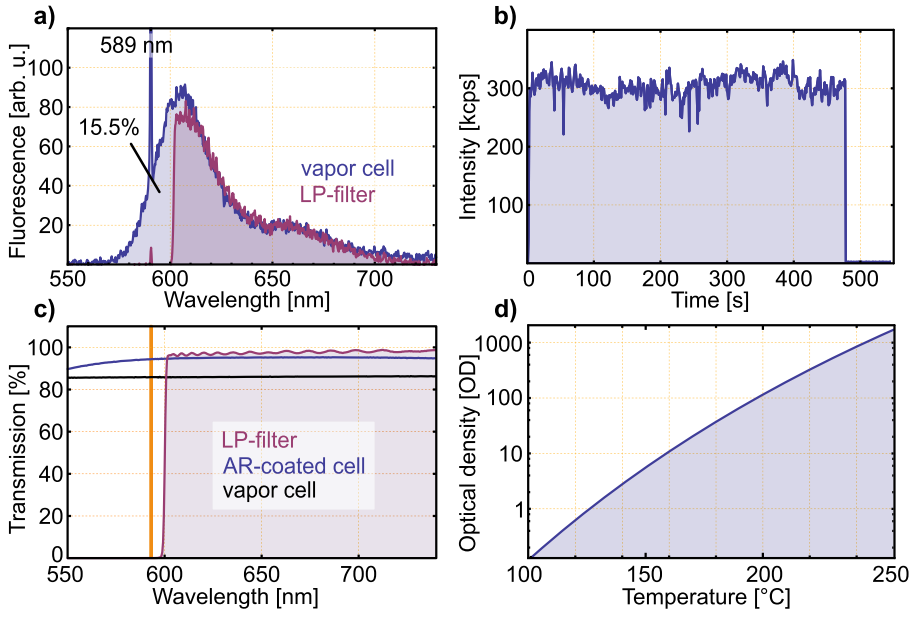

Figure 2 Relevant spectra. (a) Emission spectra of the dye Atto 590 under illumination with laser light at 589 nm, filtered solely with a hot (200°C) atomic vapor cell. Purple: Same spectrum, filtered with the commercial long-pass filter. The integral enhancement between atomic and the commercial filter is 15.5%. LP-filter = long-pass filter. **(b)** Single step bleaching of individual molecules proves the single emitter nature. **(c)** Transmission curves of the filter and different atomic vapor cells measured with a UV-VIS spectrometer (Lambda 16, PerkinElmer). **(d)** Calculated optical density of the filter (100 mm optical length) against temperature.

recorded in a commercial absorption spectrometer (PerkinElmer, Lambda 16) and is depicted in Figures 1(c) and 2(c). Please note, that this is a representation in a linear scale and the 50% point is observed around 600 nm. Even if the filter is designed to have a six to seven orders of magnitude rejection from the blue region of the spectrum to 593 nm, it is probably possible to slightly tilt the filter to blue shift its transmission closer to the excitation laser. This may result in altering the performance (transmission and rejection) of the filter and was therefore not pursued.

Alternatively, the excitation light, scattered and reflected from the sample, is blocked solely by a hot atomic vapor cell. A simple calculation [19] of the six D_2 transitions ($3^2S_{1/2} \rightarrow 3^2P_{3/2}$, three from each ground state) allows to estimate the optical density for the 100 mm long cell (30 mm diameter) as a function of the temperature (Figure 2(d)). This is an idealized picture, since we do not account for any forward scattering, non-linear or saturation effects. Furthermore, the laser is represented by a delta-peak and locked to the cross-over resonance of the sodium D_2-line. The D_2-line is generally preferred for filtering, due to its higher oscillator strength by a factor of two against the D_1-line. Nevertheless, we measure a suppression of better than 6 orders of magnitude with our filter at a temperature of 200°C, which is chosen as the operation temperature for all further experiments. The measured filter function of the sodium vapor is depicted in Figure 1(d). The optical density of about 100 represents the calculated value at this temperature. The vapor pressure at 200°C is calculated to be $\sim 10^{-4}$ mbar.

Atomic sodium tends to diffuse into the usual boro-silicate glass cell and darken the windows. Therefore, the cells were made out of quartz glass. We note that special glasses and

coatings also allow a suppression of this darkening effect [32, 33]. To enhance the transmission on the cell windows, we used commercial anti-reflection coated sodium cells (Triad technologies, Longmont, Colorado). Although unspecified, the supplied coating works well up to 200°C. In addition another batch of cells was produced in house, but without an anti-reflection coating. The transmission spectra of these cells and the commercial filter is shown in Figure 2(c). As one can see, the transmission of the anti-reflection coated cell is 7-9% higher than for the uncoated one. With the resolution of the absorption spectrometer, the GHz-wide notch filtering for sodium light is not observed.

To directly compare the two filter configurations in the microscope, both filters are mounted onto a small optical bread board, which slides on rails on the optical table. The filter configuration can therefore be switched back and forth within less than a second. The area between the filters was filled with an opaque material, such that the filter configuration can be changed during a running experiment. Furthermore, the detection path was optically shielded using a black cardboard box. To ensure a well defined convection of air inside the box, it was designed such that a laminar flow was realized from bottom to top by small holes at the bottom.

3 Results

3.1 Acquired spectra

We first compare the different spectra, acquired from a single molecule in both filter configurations. When a single molecule was identified in the confocal microscope, the spectrometer was introduced and a spectrum was acquired. Figure 2(a) shows the single molecule spectra in both filter configurations. The filtering with the atomic vapor shows the entire spectrum of the single molecule as it would be excited with a more blue wavelength. On first sight, this violates energy conservation, but most likely the more blue components are introduced by anti-Stokes processes. On the other hand, we find the spectrum acquired with the commercial 593 nm long-pass filter to be cutoff until 600 nm. Furthermore, compared to the spectrum provided by the dye producer, we find the single molecule fluorescence to be spectral shifted to the blue by about 5 nm. This is not untypical for organic dyes that their fluorescent properties critically depend on their chemical environment [34, 35].

Assuming the quantum efficiency of the single photon detector is a fixed value in the range of 570-700 nm, we can directly compare the integral contribution of the dye spectra as proportional to the detected signal on the photo detector. The result is a 15.5% higher signal with atomic filtering than with a commercial long-pass filter.

Unfortunately, although the sodium vapor filter increases the overall signal from the molecule studied, it also introduced a higher laser background. In particular we find around 20 times increased laser background even though the optical rejection is calculated to be much higher than with the commercial filter. There are two explanations for this finding: (a) the filter does not have such a high rejection due to non-linearities or saturation effects in the vapor. Or, (b), the atomic filter or some components of our setup (e.g.: laser, optical fiber, sample) spectral shifts the scattered light far enough away from the laser wavelength that it cannot be blocked. To investigate this problem, we performed simple measurements of the atomic filter with laser light via bypassing the microscope with a mirror. This resulted in a measured optical rejection of more than 6 orders of magnitude. It was necessary to perform the measurements above the saturation intensity (9.4 mW/cm^2)

to determine the optical rejection of the filter due to the weak signal. Generally, a weak laser background contribution is not relevant for the acquisition of single molecule signals, since this simply adds a constant background, as long as laser power fluctuations are not too large. Following this assumption the background can be simply subtracted.

3.2 Data analysis

In the following paragraph we introduce the protocol for data analysis. For both, the confocal and the wide-field imaging, data processing was performed as follows: Since the main goal was to compare the two filter configurations, an image was acquired with each filter at the exact same settings (excitation intensity, acquisition time, etc.). Both images were acquired with minimal time delay and usually an acquisition sequence alternating several times between the commercial filter and the atomic filter was used. To avoid additional systematic errors, for example by photobleaching or mechanical drift out of the objective plane, also the filter which was used first had been alternated from sequence to sequence. Then we compared within a sequence the directly following images. The two corresponding images were processed by an automated peak-find routine to identify the molecules. Then molecule pairs were identified by direct correlation of all emitter positions in a corresponding set of images (with the commercial and the atomic filter). The algorithm checks for the nearest neighbor in both images and saves the result with a unique pair ID. Several emitters too close to each other in one image (± 3 pixel) were not considered for further evaluations. In addition, all results (emitter pair correlations) had to be checked and confirmed manually. Each identified emitter, which belongs to a former defined pair, was then fitted by using the least-square method to a 2D-Gaussian (symmetric in x and y). The extracted fit parameters are used for further analysis. Note, that we only consider the changes we find for the directly correlated pairs. Since the molecules tend to bleach and blink at ambient conditions, this required a statistical analysis. To determine if molecules are brighter or dimmer after change the filter, we define the quantity relative enhancement ΔI as shown in equation (1):

$$\Delta I = \frac{I_{\text{vapor}} - I_{\text{comm}}}{1/2 \cdot (I_{\text{vapor}} + I_{\text{comm}})}. \tag{1}$$

In case of the confocal configuration I_{vapor} and I_{comm} are the maximum of the fitted 2D-Gaussian for the vapor cell and the commercial filter, respectively. In case of the wide-field configuration I_{vapor} and I_{comm} are the integrals of the fitted 2D-Gaussian. This is attributed to the information content of the images: In the confocal case one obtains the integrated signal from the maximum of the emitter position; whereas in the case of the wide-field one acquires a photon distribution which obeys the point spread function of the system. Subsequently, an integration of the signal is required before the total photon flux is accessible.

To estimate the background and its fluctuation, all images were analyzed in an area where no molecules were present. Due to the fact that we can analyze many more molecules than images, the statistical fluctuation is higher. With this data, a histogram of signal to background (SBR) and signal to noise (SNR) ratios can be determined. Any fluctuation in the molecules emission rate was not accounted for. Assuming a non-fluctuating background contribution, this can be simply subtracted from the original data. The anal-

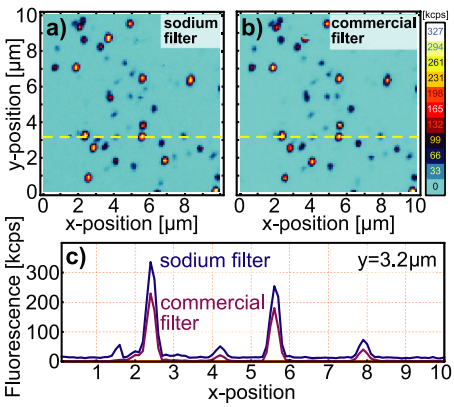

Figure 3 Confocal image of the sample. **(a)** Filtering with the atomic vapor cell (T = 200°C). The pixel size is 100 nm. The integration time per pixel is 10 ms. **(b)** Same area as before by using the commercial filter. **(c)** Line-cut of single molecules emission extracted from the above image (yellow dashed line).

ysis presented below is always a statistical comparison between both filter configurations and many co-localized single molecules.

3.3 Confocal imaging

Now we turn to the confocal configuration of the microscope. Initially, the experimental configuration was set up differently than shown in Figure 1(b): The filters were placed between the microscope and the pinhole. However, severe power fluctuations were found in the single molecule signals acquired with the atomic filter on the order of one magnitude. Due to hot air convection surrounding the vapor cell, the collimated beam wanders on the pinhole. Therefore, the confocal configuration was changed and the atomic filter was placed between the pinhole and the single photon detector. This configuration is also described in [26]. To estimate the fluctuation of the wandering beam on the detector, we placed a camera at the location of the avalanche photo diode and monitor the fluorescence of a dense labeled DNA droplet. At high speed (10 ms), a 71 µm spot size ($1/e^2$) is observed, which is the same as if no thermal fluctuations are present. With an integration over 60 s, a spot size of 82 µm is observed. The used avalanche photo diode has an active detector size of around 170 µm, so the configuration of the vapor cell behind the pinhole does not alter the performance of our setup. We experience no reduction in the spatial resolution compared to the commercial filter. For the vapor cell we find the point spread function of individual emitters to have an average full width half maximum (FWHM) of 291 nm compared to 294 nm with the commercial filter. For comparison the Airy disk should have a radius of around 277 nm for the given experimental parameters.

A raw confocal image of the single molecule sample in both filter configurations is shown in Figure 3(a) and (b). Single step blinking of a molecule is observed in the commercial filter configuration (x, y = 4, 8.5 µm). Visually, both images are comparable, but a higher background contribution around 15 kcps is observed in atomic filtering vs. very stable 2 kcps with the commercial filter. This leads to a relative increase of the background by a factor of 7.5 with the atomic filter. Subsequently, we also estimate the signal to noise ratio to be an order of magnitude larger with the commercial filter (SNR = 800!). This is different than in the experiments under cryogenic conditions [29]. The increase in excitation power at ambient conditions (µW instead of nW at cryogenic conditions) seem to have an influence on the signal to noise ratio. This could be a hint, that saturation effects in the vapor increases the background.

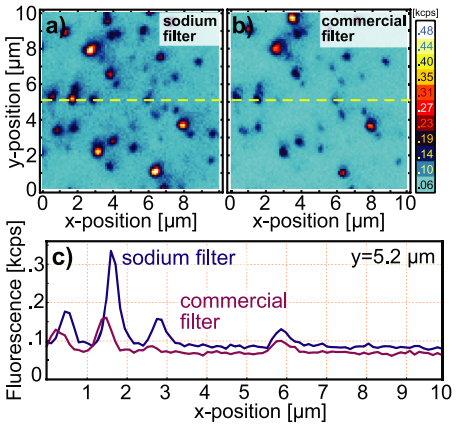

Figure 4 Wide-field image of the DNA sample. **(a)** Unter atomic filtering (T = 200°C). The acquisition time per frame is 10 s. **(b)** Same with filtering by the commercial filter. **(c)** Line-cut of a single molecule (yellow dashed line). The wide-field configuration is more sensitive to scintillations that causes temporal changes in the refractive index of the air. As a consequence the image is blurred out.

The line cuts in Figure 3(c) illustrate the background level. The image background acquired with atomic filtering is higher by a factor of 7-8 based on a laser-power of 1 µW into the microscope. This is fully consistent with the measurements of the optical density: The commercial filter shows an optical density of about seven, whereas the atomic vapor cell was determined to show six orders of magnitude optical suppression.

In an statistical analysis of 963 molecules, when each molecule is compared in both filter configurations, we observe an enhancement in the overall detected counts per emitter of 15.4% (calculated by using equation (1)). Figure 5(a) shows a histogram for all recorded molecule pairs. The statistical error defined as $\sigma/\sqrt{N}$ is 1.5%. The atomic filter therefore increases the number of collected photons, but the background suppression is one order of magnitude smaller for the vapor cell to the commercial filter.

3.4 Wide-field imaging

In the wide-field experiment no pinhole is introduced. Therefore, clipping of a wandering beam is not critical. Instead, convection of hot air originating from the vapor cell leads to a shifted or blurred image. In fact, the image is found slightly blurred. The average FWHM of the fluorescence molecules for the atomic cell is 427 nm and for the commercial filter 365 nm. Following the Rayleigh criteria this would clearly result in a reduction of the resolution for the atomic vapor cell compared to the confocal configuration. For localization spectroscopic methods [5, 6] also the number of detected photons directly influences the localization precision: For the used filters one would find a reduction of 10% compared to 17% when only considering the Rayleigh criteria. Of course, this implies that one can treat the wandering of the beam on the CCD chip as a stochastic distribution within the measurement time.

The images looks as in previous case comparable between the two filter configurations (Figure 4(a) and (b)). The background contribution in the atomic filter case is increased, but not as significant as in the confocal configuration. In an analysis of all acquired images, the mean background contribution is increased by 30% from 70 to 100 cps. This increase is also visible in the line-cut shown in Figure 4(c).

For the detection efficiency calculated by integrating over the emitters point spread function, an enhancement of 18.7% with a standard deviation of σ = 28.4% is observed. Taking 2,337 measured molecules into account, this leads to a statistical uncertainty of 0.6%. The noise level of the commercial filter and sodium filter is determined to be 30 vs.

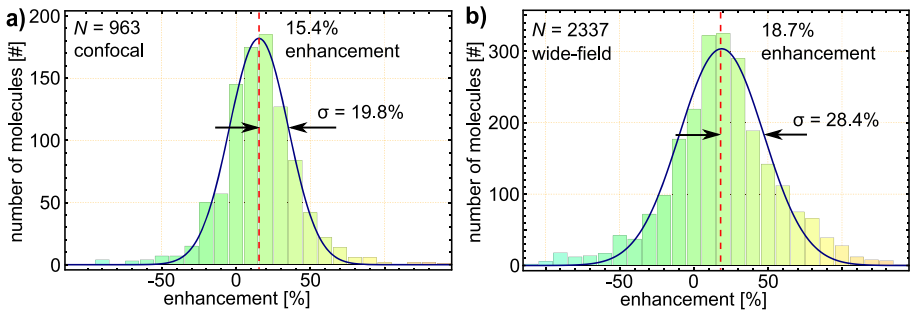

Figure 5 Direct comparison of the enhancement of multiple molecules in the different filter configurations. Molecules tend to blink and bleach, such that statistical data processing is necessary. **(a)** 963 molecules, detected in a confocal configuration. The signal for the atomic notch filter is improved by 15.4% for the atomic notch filter. *N* = number of molecules. **(b)** 2337 molecules, detected in a wide-field microscope. The enhancement is shown to be 18.7%. The statistical distribution of the enhancement is wider than in the confocal case due to the generally lower SNR than in the confocal configuration.

40 photons per seconds, based on a laser excitation of 50 μW into the microscope. The increased noise of the atomic filter tends to lower the SNR. However, the higher signal not only compensates this drawback, but gives an increase in the SNR. We find an SNR of 60 for atomic filtering vs. 31 with the commercial filter. The intrinsic noise level of the camera is at least one order of magnitude less and does not play a role here. In summary, we achieve an increased signal, as well as an increased signal to noise ratio for the atomic filter vs. the commercial filter in the wide-field imaging configuration.

3.5 Overall enhancement

Figure 5 shows a histogram of the determined integrated count rates for the commercial and the atomic filtering schemes. Molecules tend to blink and bleach and it is possible that a molecule was fully bright in one image and much dimmer in the next image, acquired with the other filter. The higher fluctuation on the camera (wandering image) leads to an increased spread of the resulting count rate. Therefore, a much wider distribution than in the confocal case is observed. Another important factor is the signal to noise ratio (SNR) in the analyzed image. When e.g. the background noise in the image is higher, the resulting fit outcome for a single molecule shows higher fluctuations. Thereby, Figure 5 does not only represent the overall enhancement of the signal, but also represents the SNR.

In summary, the confocal images show a lower SNR and SBR for an atomic vapor cell filter compared to a commercial filter. But the lateral spread of the molecules does not change and we find an enhancement in the total number detected photons of $15.4 \pm 1.5\%$.

The wide-field images show a comparable SBR for both filters. For wide-field applications the vapor-cell filter exhibits a better detection efficiency than the commercial filter by $18.7 \pm 0.6\%$ for the total detected signal and a factor two increased SNR.

In both configurations, atomic filtering results in an enhancement of the number of detectable photons on the order of 15%. This is fully consistent with the single molecule spectra as shown in Figure 2(a), which also indicate an overall enhancement of approximately 15%.

4 Conclusion and outlook

The atomic notch filter poses an alternative to commercial available filters. The improvement of about 15% is accounted to rejecting solely the laser, while allowing the entire fluorescence spectrum of the emitter to pass the filter. This also allows for studies on weakly spectral shifted signals against the excitation wavelength. This can be a crucial enhancement for microscopy and sensing. It allows for studies on low fluorescing samples down to the single molecule level. The increased background fluctuations in the confocal case need to be addressed, eventually with a widened beam to lower the intensity inside the vapor cell. Also a filter cavity should be used to clean up the laser light leaving the fiber. In Raman spectroscopy, atom-based narrow-band filters were explored in the near-infrared part of the spectrum [26], but such experiments were not performed with atomic sodium and yellow light. We underline that the introduced sodium filter matches well to many dyes used in (micro-)biological imaging. So far, other vapor cells, such as Cs, Rb, have been subject for study. Such filters can allow for the sensitive detection of weakly fluorescing defect centers, such as defects in silicon-carbide [36], which could be eventually combined with e.g. atomic rubidium or cesium.

The experimental challenges of using atomic vapor cells are not necessarily easy to solve in micro-biology labs. However, the introduced filtering option allows for enhancing the overall collection efficiency after everything else has been optimized. A complementary feature to this atomic notch filter is the use of a Faraday anomalous dispersion optical filter (FADOF), which represents a GHz-wide band-pass configuration [37, 38]. In the future, when convenient diode lasers operating at the sodium wavelength are available, the technique of filtering a single molecule with an atomic vapor notch may give a small but crucial enhancement of detection efficiency, which in turn would allow better sensing and localization accuracies in material-science and applications in micro-biology.

Competing interests
The authors declare no competing financial interests.

Authors' contributions
IG envisioned and prepared the experiments. TR helped with the configuration and the design of the microscope. DU and TR performed the measurements. IG, DU, TR, and MW processed the data. JW, SL and IG supervised the team. IG, MW and TR wrote the manuscript.

Acknowledgements
We thank Andrea Zappe for DNA preparation and Helmut Kammerlander from the glass shop for producing several sodium cells. We also thank Philip Hemmer and Nathan Chejanovsky for carefully proofreading the manuscript. Initial experiments were conducted by Guilherme Stein & Petr Siyushev. We acknowledge funding from the Max Planck Society (JW, Max Planck fellowship).

Received: 26 February 2015 Accepted: 10 August 2015 Published online: 26 August 2015

References

1. Hirschfeld T. Optical microscopic observation of single small molecules. Appl Opt. 1976;15(12):2965-6. doi:10.1364/AO.15.002965.
2. Moerner W, Kador L. Optical detection and spectroscopy of single molecules in a solid. Phys Rev Lett. 1989;62(21):2535-8. doi:10.1103/PhysRevLett.62.2535.
3. Orrit M, Bernard J. Single pentacene molecules detected by fluorescence excitation in a *p*-terphenyl crystal. Phys Rev Lett. 1990;65:2716-9. doi:10.1103/PhysRevLett.65.2716.
4. Hell SW, Stelzer EHK, Lindek S, Cremer C. Confocal microscopy with an increased detection aperture: type-B 4Pi confocal microscopy. Opt Lett. 1994;19:222-4. doi:10.1364/OL.19.000222.
5. Betzig E, Patterson GH, Sougrat R, Lindwasser OW, Olenych S, Bonifacino JS, Davidson MW, Lippincott-Schwartz J, Hess HF. Imaging intracellular fluorescent proteins at nanometer resolution. Science. 2006;313(5793):1642-5. doi:10.1126/science.1127344.
6. Rust MJ, Bates M, Zhuang X. Sub-diffraction-limit imaging by stochastic optical reconstruction microscopy (storm). Nat Methods. 2006;3(10):793-6. doi:10.1038/nmeth929.

7. Schafer D, Gelles J, Sheetz M, Landick R. Transcription by single molecules of RNA polymerase observed by light microscopy. Nature. 1991;352(6334):444-8. doi:10.1038/352444a0.
8. Nie S, Chiu D, Zare R. Probing individual molecules with confocal fluorescence microscopy. Science. 1994;266(5187):1018-21. doi:10.1126/science.7973650.
9. Nie S, Zare RN. Optical detection of single molecules. Annu Rev Biophys Biomol Struct. 1997;26(1):567-96. doi:10.1146/annurev.biophys.26.1.567.
10. Weiss S. Fluorescence spectroscopy of single biomolecules. Science. 1999;283(5408):1676-83. doi:10.1126/science.283.5408.1676.
11. Gordon MP, Ha T, Selvin PR. Single-molecule high-resolution imaging with photobleaching. Proc Natl Acad Sci USA. 2004;101(17):6462-5. doi:10.1073/pnas.0401638101.
12. Jelezko F, Tietz C, Gruber A, Popa I, Nizovtsev A, Kilin S, Wrachtrup J. Spectroscopy of single N-V centers in diamond. Single Mol. 2001;2:255-60. doi:10.1002/1438-5171(200112)2:4<255::AID-SIMO255>3.0.CO;2-D.
13. Vlasov II, Shiryaev AA, Rendler T, Steinert S, Lee S-Y, Antonov D, Voros M, Jelezko F, Fisenko AV, Semjonova LF, Biskupek J, Kaiser U, Lebedev OI, Sildos I, Hemmer PR, Konov VI, Gali A, Wrachtrup J. Molecular-sized fluorescent nanodiamonds. Nat Nanotechnol. 2014;9(1):54-8. doi:10.1038/nnano.2013.255.
14. Biju V, Itoh T, Anas A, Sujith A, Ishikawa M. Semiconductor quantum dots and metal nanoparticles: syntheses, optical properties, and biological applications. Anal Bioanal Chem. 2008;391(7):2469-95. doi:10.1007/s00216-008-2185-7.
15. Sandoghdar V, Klotzsch E, Jacobsen V, Renn A, Hakanson U, Agio M, Gerhardt I, Seelig J, Wrigge G. Optical detection of very small nonfluorescent nanoparticles. Chimia. 2006;60:761-4. doi:10.2533/chimia.2006.761.
16. Gerhardt I, Wrigge G, Hwang J, Zumofen G, Sandoghdar V. Coherent nonlinear single molecule microscopy. Phys Rev A. 2010;82:063823. doi:10.1103/PhysRevA.82.063823. http://journals.aps.org/pra/abstract/10.1103/PhysRevA.82.063823.
17. Lee KG, Chen WX, Eghlidi H, Kukura P, Lettow R, Renn A, Sandoghdar V, Götzinger S. A planar dielectric antenna for directional single-photon emission and near-unity collection efficiency. Nat Photonics. 2011;5(3):166-9. doi:10.1038/nphoton.2010.312.
18. Jamali M, Gerhardt I, Rezai M, Frenner K, Fedder H, Wrachtrup J. Microscopic diamond solid-immersion-lenses fabricated around single defect centers by focused ion beam milling. Rev Sci Instrum. 2014;**85**(12). doi:10.1063/1.4902818.
19. Domenico GD, Weis A. Spectra of the D-lines of alkali vapors. Wolfram Demonstrations Project. 2011. http://demonstrations.wolfram.com/SpectraOfTheDLinesOfAlkaliVapors/.
20. Heifetz A, Agarwal A, Cardoso GC, Gopal V, Kumar P, Shahriar MS. Super efficient absorption filter for quantum memory using atomic ensembles in a vapor. Opt Commun. 2004;232(1-6):289-93. doi:10.1016/j.optcom.2004.01.006.
21. Weller L, Kleinbach KS, Zentile MA, Knappe S, Adams CS, Hughes IG. Absolute absorption and dispersion of a rubidium vapour in the hyperfine Paschen-Back regime. J Phys B, At Mol Opt Phys. 2012;45(21):215005. doi:10.1088/0953-4075/45/21/215005.
22. Camparo J. The rubidium atomic clock and basic research. Phys Today. 2007;60(11):33-9. doi:10.1063/1.2812121.
23. Pelletier MJ. Ultraviolet Raman spectroscopy using an atomic vapor filter and incoherent excitation. Appl Spectrosc. 1992;46(3):395-400. doi:10.1366/0003702924125320.
24. Chen H, White MA, Krueger DA, She CY. Daytime mesopause temperature measurements with a sodium-vapor dispersive Faraday filter in a lidar receiver. Opt Lett. 1996;21(15):1093-5. doi:10.1364/OL.21.001093.
25. Junxiong T, Qingji W, Yimin L, Liang Z, Jianhua G, Minghao D, Jiankun K, Lemin Z. Experimental study of a model digital space optical communication system with new quantum devices. Appl Opt. 1995;34(15):2619-22. doi:10.1364/AO.34.002619.
26. Lin J, Li Y-Q. Ultralow frequency Stokes and anti-Stokes Raman spectroscopy of single living cells and microparticles using a hot rubidium vapor filter. Opt Lett. 2014;39(1):108-10. doi:10.1364/OL.39.000108.
27. Minsky M. Microscopy apparatus. 1961. http://worldwide.espacenet.com/publicationDetails/biblio?CC=US&NR=3013467&KC=&FT=E&locale=en_EP.
28. Singer E. A microscope for observation of fluorescence in living tissues. Science. 1932;75(1941):289-91. doi:10.1126/science.75.1941.289-a.
29. Siyushev P, Stein G, Wrachtrup J, Gerhardt I. Molecular photons interfaced with alkali atoms. Nature. 2014;509(7498):66-70. doi:10.1038/nature13191.
30. Lee Y-H, Maus RG, Smith BW, Winefordner JD. Laser-induced fluorescence detection of a single molecule in a capillary. Anal Chem. 1994;66:4142-9. doi:10.1021/ac00095a005.
31. Petelski T, Fattori M, Lamporesi G, Stuhler J, Tino GM. Doppler-free spectroscopy using magnetically induced dichroism of atomic vapor: a new scheme for laser frequency locking. Eur Phys J, D, At Mol Opt Phys. 2003;22(2):279-83. doi:10.1140/epjd/e2002-00238-4.
32. Laux L, Schulz G. A sodium-resistant glass cell by coating with caf 2. J Phys E, Sci Instrum. 1980;13(8):823.
33. Sakurai T, Tanaka K, Miyazaki H, Ichimoto K, Sakata A, Wada S. Construction of long-life magneto-optical filters for helioseismology observations. In: Osaki Y, Shibahashi H, editors. Progress of seismology of the sun and stars. Lecture notes in physics vol. 367. Berlin: Springer; 1990. p. 277-80. doi:10.1007/3-540-53091-6_92.
34. Kubin RF, Fletcher AN. Fluorescence quantum yields of some rhodamine dyes. J Lumin. 1983;27(4):455-62. doi:10.1016/0022-2313(82)90045-X.
35. Arbeloa FL, Aguirresacona IU, Arbeloa IL. Influence of the molecular structure and the nature of the solvent on the absorption and fluorescence characteristics of rhodamines. Chem Phys. 1989;130(1-3):371-8. doi:10.1016/0301-0104(89)87066-1.
36. Widmann M, Lee S-Y, Rendler T, Son NT, Fedder H, Paik S, Yang L-P, Zhao N, Yang S, Booker I, Denisenko A, Jamali M, Momenzadeh SA, Gerhardt I, Ohshima T, Gali A, Janzén E, Wrachtrup J. Coherent control of single spins in silicon carbide at room temperature. Nat Mater. 2015;14(2):164-8. doi:10.1038/nmat4145.
37. Dick DJ, Shay TM. Ultrahigh-noise rejection optical filter. Opt Lett. 1991;16(11):867-9. doi:10.1364/OL.16.000867.
38. Kiefer W, Löw R, Wrachtrup J, Gerhardt I. Na-Faraday rotation filtering: the optimal point. Sci Rep. 2014;4:6552. doi:10.1038/srep06552.